Eddy current studies for the beam screen of the Electron-Ion Collider hadron storage ring superconducting magnets

S. Verdu-Andres

September 2022

Electron-Ion Collider

Brookhaven National Laboratory

U.S. Department of Energy

DISCLAIMER

Eddy current studies for the beam screen
of the Electron-Ion Collider hadron storage ring superconducting magnets

Silvia Verdú-Andrés* and Holger Witte

Brookhaven National Laboratory
Upton, NY 11973 (USA)

(Dated: September 30, 2022)

A copper-clad stainless steel beam screen will be installed in each of the Relativistic Heavy Ion Collider (RHIC) superconducting (SC) magnets used for making the Electron-Ion Collider (EIC) Hadron Storage Ring (HSR). Eddy currents are induced within conductors to oppose a changing magnetic flux. Eddy currents will appear on the EIC HSR beam screens during ramp up and ramp down, after a magnet quenches and when reversing the polarity of the γ transition jump quadrupoles during γ transition crossing. This study evaluates the magnitude of the eddy currents, the temperature increase due to Joule heating and the stress at the beam screens from the eddy-current induced force.

I. MOTIVATION

Eddy currents are induced within metals to oppose a changing magnetic flux, as explained by the Lenz's law, with larger eddy currents appearing in metals with lower electrical resistivity. Adverse effects of the induced eddy currents include Joule heating, Lorentz forces and superimposing magnetic fields delayed in time with respect to the time-varying magnetic field which originated the eddy currents.

A beam screen will be installed in each of the RHIC SC magnets used for the EIC HSR [1]. The beam screens are made from copper-clad stainless steel sheets with a 75 µm thick high Residual Resistive Ratio (RRR) copper layer on top of a 1 mm-thick 316LN stainless steel layer [2]. The screens will be actively cooled with helium and kept between 4.55 and 10 K during beam operation. Eddy currents will be induced in the beam screen during magnetic field ramp up and ramp down and as a result of a magnet quench. The magnitude of the eddy currents depends on the beam screen design and the time variation of the magnetic field. The ramp up and ramp down of the RHIC SC magnets is much slower (few tens of A per second, as shown in Fig. 2 of Ref. [3]) than the current decay from a magnet quench (kA per second), so the main focus is set on the eddy currents appearing as a result of a magnet quench. Special attention is paid to the eddy currents in the beam screens of the RHIC γ transition jump quadrupoles. In RHIC all the particle species except for the protons need to cross γ transition during acceleration [4]. This will also be the case for the EIC HSR. Fast γ transition crossing is key to prevent beam losses and emittance blow up. The γ transition crossing scheme for RHIC (and the future EIC HSR) requires a series of γ transition jump quadrupoles to change their polarity in about 40 ms [5–7] (few kA per second, as shown in Fig. 1 and sketched in Fig. 2 of Ref. [8]).
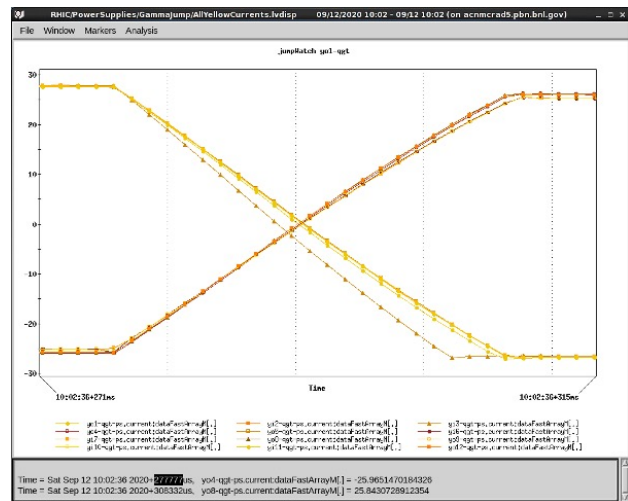

FIG. 1. Polarity reversal of γ transition jump quadrupoles implemented during γ transition crossing at RHIC. [Image courtesy of Aljosa Marusic (BNL).]

The induced magnetic field resulting from the eddy currents will superpose the original time-varying magnetic field, with the metallic pipe effectively shielding the original magnetic field. For an electrically thin cylindrical metallic pipe embedded in a time-varying dipole field $B_0(t) = B\sin(\omega t)$, the magnetic field seen in the pipe will be [9, 10]:

$$B(t) = \frac{B}{\sqrt{1 + (\omega\tau)^2}} \sin\left[\omega t - \arctan(\omega\tau)\right] \qquad (1)$$

where $\tau = \mu_0 bt/2\rho$ is the inverse of the cutoff angular frequency $\omega_c = 2\pi f_c$, μ_0 is the vacuum permeability, ρ is the direct-current (DC) electrical resistivity of the beam pipe, b is the beam pipe radius and t is the beam pipe thickness. The term $1 + (\omega\tau)^2$ damps the field response; the term $\arctan(\omega\tau)$ introduces a delay. Both delay and damping are larger for fast-changing fields (ω), good conductors ($1/\rho$), thick shields (t) and larger pipes (b).

---
* sverdu@bnl.gov (corresponding author)

Eddy currents in the stainless steel beam pipes of the RHIC SC magnets are negligible given the large electrical resistivity of the stainless steel. The main concern is raised by the beam screens, given the high electrical conductivity of their copper layer – especially at cryogenic temperatures. The shielding cutoff frequency for the beam pipe at the RHIC arcs, with an inner diameter of 69 mm, is about kHz and should have no impact on the γ transition jump quadrupole fields. With a beam screen of the same diameter (assumed round, with 75 µm RRR=100 copper on top of 1 mm stainless steel at 10 K, no perforations), the cutoff may be as low as 10 Hz and could increase the time it takes to reverse polarity in the γ transition crossing jump quadrupoles and/or reduce the final strength of the field seen by the beam. Fig. 2 shows the Bode plot for both scenarios. The response of the multilayer screen is estimated by assuming an equivalent electrical conductivity that results from weighting the conductivity of each layer with their thickness.
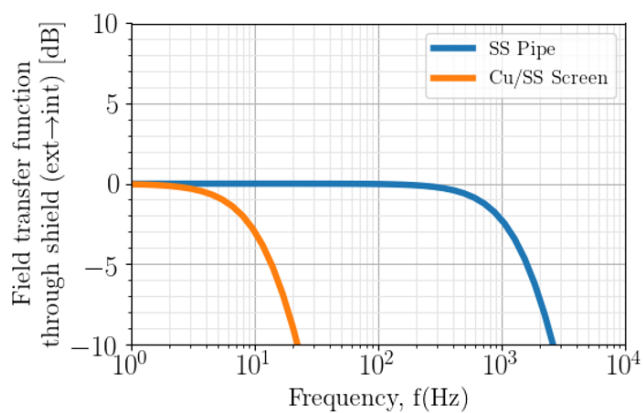

FIG. 2. Frequency response for the transfer function of a time-varying magnetic field through the current RHIC beam pipe and the planned EIC HSR beam screen.

The next sections discuss the impact of eddy currents on I) the beam screens of the RHIC arc dipoles during magnet quench, and II) the beam screens located in the RHIC γ transition jump quadrupoles during polarity reversal. The studies assume a negligible effect of the pumping slots on the eddy currents.

II. CASE I: ARC DIPOLES

The eddy currents induced in the walls of a cylindrical metallic pipe by a time-varying magnetic field will exert a force on the pipe walls that is proportional to the magnetic field and its variation with time [11, 12]:

$$\frac{d^2F}{d\varphi dz} \propto b^2 B(t)\frac{dB(t)}{dt} \qquad (2)$$

COMSOL [13] simulations are used to evaluate the expected deformation and stresses in the beam screen as result of the quench-induced eddy current forces that will appear on the screen after a RHIC arc dipole quenches. The simulations assume a maximum $B(t) \times dB(t)/dt$ of -30 T^2/s. This is a conservative value observed for quenches of RHIC arc dipoles in the BNL's Magnet Division test bench (see Fig. 3), in comparison to the slower rates registered for beam quenches in RHIC, where each dipole is equipped with a quench protection diode that by-passes the current from the other SC magnets in the string while the magnet is quenching. The modelled screen has a 75 µm-thick RRR=100 copper layer on top of a 0.5 mm-thick stainless steel layer at 10 K, which 2D profile is shown in Fig. 6. The COMSOL simulation uses typical values at room temperature for the Young's modulus (σ) and Poisson's ratio (μ) of the copper and stainless steel layers listed in Table I and assumes a linear strain-stress dependency.
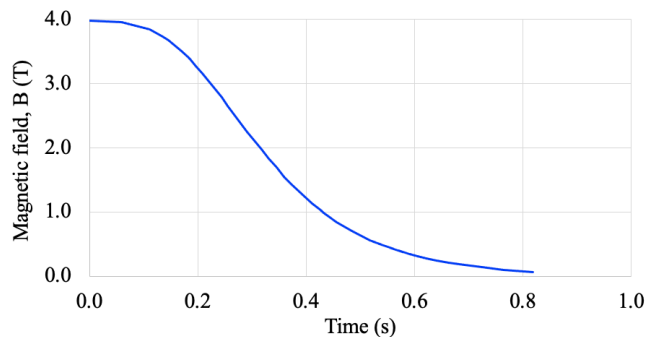

FIG. 3. Magnetic field decay after quench of a RHIC arc dipole as recorded during the BNL's Magnet Division bench tests. The transfer function correlating magnetic field and current intensity for a typical arc dipole is found in Ref. [14]. [Data facilitated by Joseph Muratore (BNL).]

Layer	Young's modulus σ (GPa)	Poisson's ratio μ
Copper	110	0.35
Stainless steel	205	0.28

TABLE I. Material properties applied to the copper and stainless steel layers of the screen for COMSOL simulations.

Simulations show that the maximum expected displacement is less than 1 µm – negligible – and the stresses are 5 MPa maximum – well below the yield strength of copper and stainless steel at cryogenic temperatures [15]. Fig. 5 shows the evolution of the von Mises stress with time after arc dipole quench calculated by COMSOL for a constant, linear variation of the magnetic field with time of 8 T/s, so that the maximum value of the product $B(t) \times dB(t)/dt$ provided by the modeled $B(t)$ shown in Fig. 4 used for the simulation is comparable to the derived from the measured $B(t)$ in Fig. 3. Fig. 6 shows the deformation and von Mises stress that the quench-

induced eddy current forces inflict on the beam screen 0.1 seconds after the arc dipole quench and Fig. 7 provides a close view of the von Mises stress for the two layers of the beam screen. The maximum displacement is experienced by the rounded walls of the beam screen and found at the equatorial plane. The point displaces outwards by 0.32 µm. The stainless steel layer concentrates higher stresses than the copper layer. The maximum stress in the beam screen is 20 MPa, below the yield strength of copper [16] and stainless steel [17].
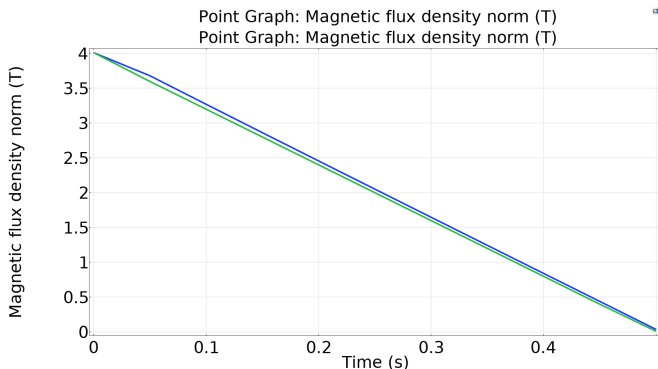

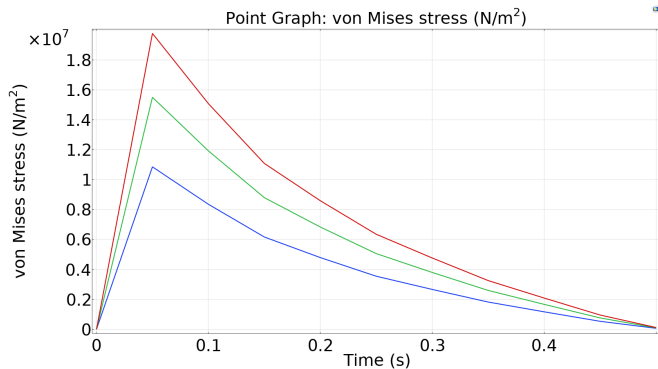FIG. 4. Time evolution of magnetic field after quench used as an input for the COMSOL simulation.

FIG. 5. Evolution of von Mises stress with time after arc dipole quench.

III. CASE II: GAMMA TRANSITION JUMP QUADRUPOLES

An electrically thin metallic round beam pipe embedded in a time-varying quadrupolar magnetic field $K_0(t) = K_0 \sin(\omega t)$ will shield the field, with the resulting field inside the pipe being:

$$K(t) = \frac{K_0}{\sqrt{1 + \left(\frac{\omega\tau}{2}\right)^2}} \sin\left(\omega t - \arctan\left(\frac{\omega\tau}{2}\right)\right) \quad (3)$$
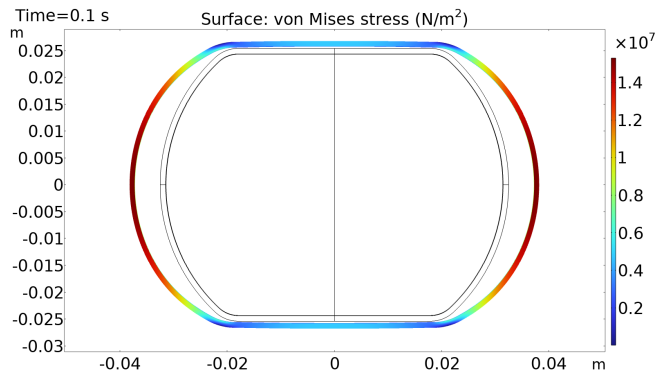

FIG. 6. Displacement of beam screen walls (2430:1 scale, in color) with respect to the nominal shape (in black) and associated von Mises stress 0.1 seconds after arc dipole quench.
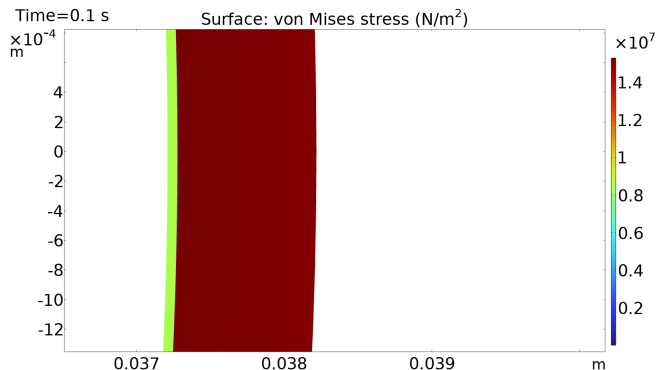

FIG. 7. Detail of von Mises stress for the two layers of the beam screen at the horizontal plane 0.1 seconds after arc dipole quench.

The corresponding impulse response or Green function $g(t)$ in t-domain, which has a Fourier transform $G(\omega)$ in ω-domain [1], is:

$$g(t) = H(t)\frac{e^{-2t/\tau}}{\tau/2} \xrightarrow{Fourier} G(\omega) = \frac{1}{1 + i\omega\tau/2} \quad (4)$$

where $H(t)$ is the Heaviside function. Fig. 8 shows the transfer function of a quadrupole field for a round, 35 mm-radius, 75 µm-thick tube made of RRR=100 copper at 10 K calculated using Eq. 3 and fitted to the function from Eq. 4. The calculation assumes that the field response is dominated by the high RRR copper layer, which exhibits significantly low electrical resistivity at cryogenic temperatures, and in consequence neglects the effect of the stainless steel beam pipe as well as the thin amorphous carbon and the stainless steel layers of the screen. The parameter τ is few ms, of the same order of magnitude as the desired time to change the polarity of the γ transition jump quadrupoles. This result suggests that the cold copper layer in the beam screen of the γ transition jump quadrupoles will likely impact the field seen by the beam during the polarity reversal.
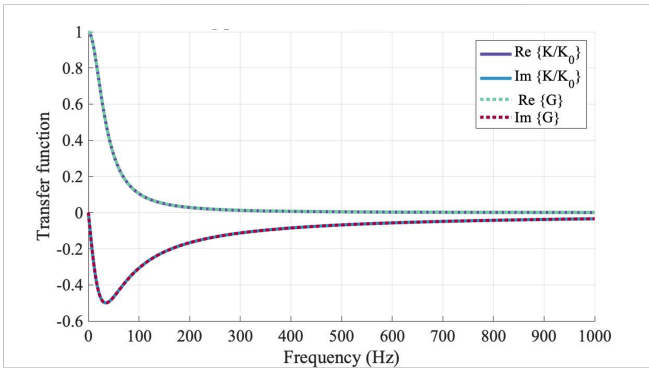
FIG. 8. Transfer function of quadrupole field for round, 35 mm-radius, 75 µm-thick tube made of RRR=100 copper at 10 K. K/K_0 is calculated using Eq. 3 and $G(\omega)$ is in Eq. 4.

The smoothing exponential, with a known Fourier transform provided in Eq. 4, is then used to calculate the field that the beam will see as a result of the eddy currents appearing due to the time-varying magnetic field shown in Fig. 9. The impact of the screen on the field amplitude is negligible as shown in Fig. 10, but modifies the slew rate significantly (a full polarity reversal takes much longer than the required 40 ms), what may compromise the desired fast γ transition crossing. The slew rate becomes slower for larger RRR values.
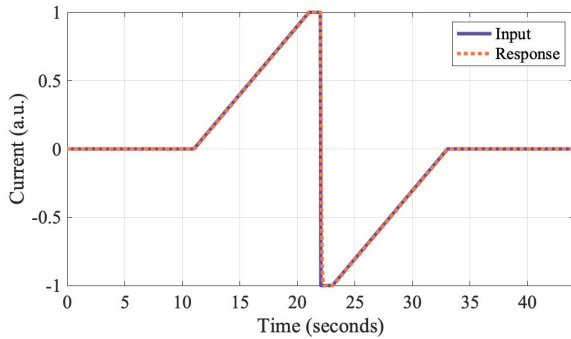

FIG. 9. Modeled time-varying signal applied to the γ transition jump quadrupoles (purple, solid line) and response calculated using Eq. 4 for a round, 35 mm-radius, 150 µm-thick tube made of RRR=100 copper at 10 K (orange, dotted line). Zoom in on the response signal shown in Fig. 10.

The planned solution is to minimize the eddy currents by introducing slots that interrupt the copper layer such that the magnetic-field time-varying induced eddy currents travel through a path with increased electrical resistance – the stainless steel layer. For an infinitely long beam screen, the eddy currents travel in the longitudinal direction along the length of the screen. The slots have to be perpendicular to the expected eddy currents, that is, lay in the azimuthal coordinate to mitigate the eddy currents.

COMSOL [13] simulations evaluate the magnitude of the eddy currents and their path, the resulting forces ex-
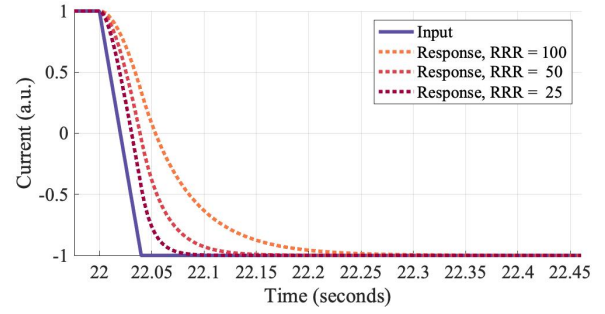

FIG. 10. Zoom in on the response for the time-varying quadrupole field shown in Fig. 9 in a round, 35 mm-radius, 150 µm-thick tube made of RRR copper at 10 K.

erted on each layer of the screen, and the associated Joule heating and consequent temperature increase. The simulations involve a polygonal screen as shown in Fig. 11 with a stainless steel cooling pipe. The screen is made of a bi-layer sheet with a 75 µm thick RRR=100 copper on top of a 0.5 mm-thick 316LN stainless steel layer. Material properties from cryogenic to room temperatures are taken from the NIST cryogenic material properties database [18]. The screen model is 10 mm long, with a slot or gap interrupting the copper layer along the full azimuth at its center. In RHIC, the relativistic gamma at transition γ_T is about 23.3 for Au ions, which corresponds to a beam rigidity $B\rho$ of 180.5 Tm and the focusing gradient of the γ transition jump quadrupoles is varied from 0.764 T/m to -0.764 T/m in about 40 ms. This is the field variation implemented in the simulations.
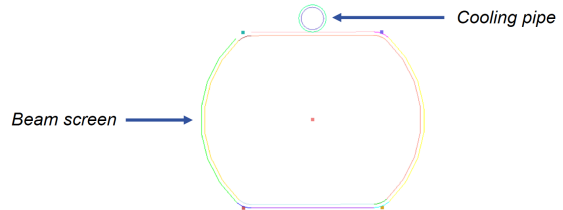

FIG. 11. Transverse cross-section of the simulated screen.

The computed eddy current flows through the least resistive path, from the top flat section of the screen along the slot towards the intersection between the slot and the horizontal plane, where finally travels through the stainless steel layer, as shown in Fig. 12. The maximum current density is 35 A/mm^2. The power dissipated by the currents is only about 2 mW per slot, with a maximum temperature increase localized at the intersection of the slot with the horizontal plane, in the stainless steel layer, that is less than few tens of mK, as illustrated in Fig. 13. The eddy current induced forces are less than 0.01 N in any of the three planes. These results confirm the solution's feasibility to mitigate the effects of eddy currents in the screens of the γ transition jump quadrupoles dur-

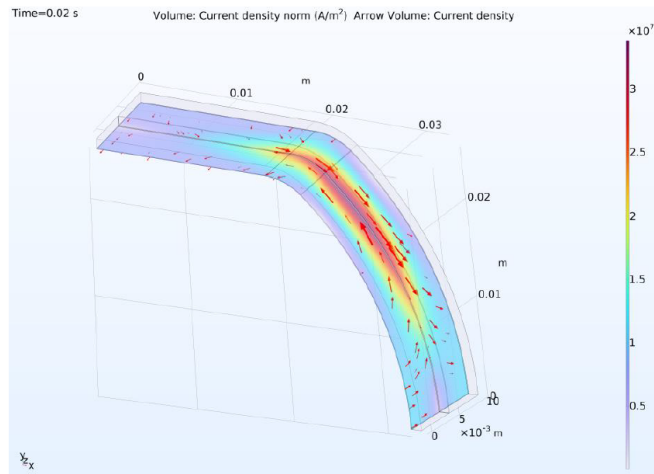ing the transition crossing and guarantee a fast transition crossing.

FIG. 12. Eddy current distribution in the surroundings of the slot. Only a quarter of the screen is depicted.
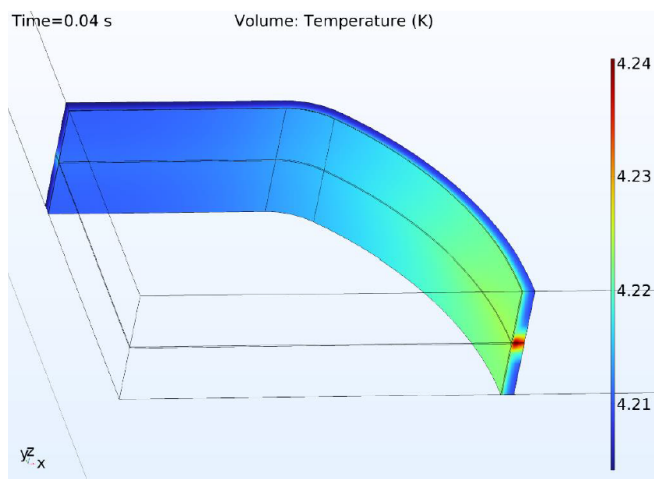

FIG. 13. Temperature distribution in the surroundings of the slot. Only a quarter of the screen is depicted.

IV. SUMMARY AND CONCLUSIONS

This note examined the impact on eddy currents on the beam screens that will be installed in the RHIC superconducting magnets used for the EIC HSR. The focus was set on the quench-induced eddy currents appearing in the beam screens of the RHIC arc dipoles and the eddy currents induced in the beam screens of the γ transition jump quadrupoles during polarity reversal for fast transition crossing.

COMSOL simulations for the beam screen in the RHIC arc dipoles found, for conservative values of the magnetic field decay, negligible deformation of the beam screen and

low stresses well below the yield strength of the beam screen materials. Our estimates found that the eddy currents induced in the beam screens of the γ transition jump quadrupoles would compromise the necessary fast transition crossing. The planned solution is to make transverse slots in the copper layer to mitigate the eddy currents. COMSOL simulations showed that this is a feasible solution.

[1] F. Willeke and et al., *Electron Ion Collider Conceptual Design Report*, Tech. Rep. (Brookhaven National Laboratory, 2021).

[2] S. Verdú-Andrés, J. Brennan, M. Blaskiewicz, X. Gu, R. Gupta, A. Hershcovitch, M. Mapes, G. McIntyre, J. Muratore, S. Nayak, S. Peggs, V. Ptitsyn, R. Than, J. Tuozzolo, and D. Weiss, A beam screen to prepare the RHIC vacuum chamber for EIC hadron beams: Conceptual design and requirements, in *Proc. 12th Int. Particle Acc. Conf.*, edited by JACoW (JACoW, 2021) pp. 2066–2069.

[3] C. Liu, D. Bruno, A. Marusic, M. Minty, P. Thieberger, and X. Wang, Mitigation of persistent currents. effects in the RHIC superconducting magnets, in *International Particle Accelerator Conference (IPAC'19)*.

[4] *RHIC Configuration Manual*, Tech. Rep. (Brookhaven National Laboratory, 2006).

[5] S. T. D. Peggs, S; Tepikian, A first order matched transition jump at RHIC, in *Int. Part. Acc. Conference*, edited by JACoW (JACoW, Washington, DC (United States), 1993).

[6] M. Harrison, S. Peggs, and T. Roser, The rhic accelerator, *Annual Review of Nuclear and Particle Science* **52**, 425 (2002).

[7] C. Montag and J. Kewisch, Commissioning of a first-order matched transition jump at the brookhaven relativistic heavy ion collider, *Phys. Rev. ST Accel. Beams* **7**, 011001 (2004).

[8] J. Mi, G. Ganetis, W. Louie, D. Bruno, G. Heppner, J. Sandberg, R. Zapasek, and W. Zhang, Rhic gamma transition jump power supply prototype test, in *Proceedings of the 2001 Particle Accelerator Conference* (2001).

[9] B. Podobedov, L. Ecker, D. Harder, and G. Rakowsky, Eddy Current Shielding by Electrically Thick Vacuum Chambers, in *Particle Accelerator Conference (PAC 09)* (2009) p. TH5PFP083.

[10] R. Shafer, *Eddy Currents, Dispersion Relations, and Transient Effects in Superconducting Magnets, FERMILAB-TM-0991*, Tech. Rep. (Fermi National Accelerator Laboratory, 1980).

[11] G. López, *Temperature rise in the beam tube during quench due to eddy currents and related effects*, Tech. Rep. SSCL-295 (Superconducting Super Collider Laboratory, Dallas, TX, 1990).

[12] C. Rathjen, *Bending Moment, Stresses, and Deformations of Beam Screens in a Quadrupole Field During Quench*, Tech. Rep. LHC-VAC/CR Vacuum Technical Note 02-13 (CERN, Geneva (Switzerland), 2002).

[13] COMSOL, https://www.comsol.com (2022).

[14] M. Anerella, J. Cottingham, J. Cozzolino, P. Dahl, Y. Elisman, J. Escallier, H. Foelsche, G. Ganetis, M. Garber, A. Ghosh, C. Goodzeit, A. Greene, R. Gupta, M. Harrison, J. Herrera, A. Jain, S. Kahn, E. Kelly, E. Killian, M. Lindner, W. Louie, A. Marone, G. Morgan, A. Morgillo, S. Mulhall, J. Muratore, S. Plate, A. Prodell, M. Rehak, E. Rohrer, W. Sampson, J. Schmalzle, W. Schneider, R. Shutt, G. Sintchak, J. Skaritka, R. Thomas, P. Thompson, P. Wanderer, and E. Willen, The rhic magnet system, *Nuclear Instruments and Methods in Physics Research Section A: Accelerators, Spectrometers, Detectors and Associated Equipment* **499**, 280 (2003), the Relativistic Heavy Ion Collider Project: RHIC and its Detectors.

[15] J. Polinski, Materials in cryogenics, *European course in cryogenics*, CERN, Geneva (Switzeland): https://indico.cern.ch/event/90787/sessions/113900/attachments/1093424/1559936/Materials_in_Cryogenics.pdf (2010).

[16] Cryogenic Properties of Copper, https://www.copper.org/resources/properties/144_8/ (Last accessed: 2022-09-29).

[17] Materials for cryogenic service: engineering properties of austenitic stainless steels, https://nickelinstitute.org/media/1723/materialsforcryogenicservice_engineeringpropertiesofausteniticstainlesssteel_4368_.pdf, last accessed: 2022-09-29.

[18] NIST properties of solid materials from cryogenic-to room-temperatures, https://trc.nist.gov/cryogenics/materials/materialproperties.htm (Last accessed: 2022-08-12).